THE JOURNAL OF PHYSICAL CHEMISTRY C

Article

pubs.acs.org/JPCC

Mechanosynthesis of the Fast Fluoride Ion Conductor $Ba_{1-x}La_xF_{2+x}$: From the Fluorite to the Tysonite Structure

A. Düvel,*[,†] J. Bednarcik,[‡] V. Šepelák,[§] and P. Heitjans*[,†]

[†]Institute of Physical Chemistry and Electrochemistry, and ZFM – Center for Solid State Chemistry and New Materials, Leibniz University Hannover, Callinstr. 3-3a, 30167 Hannover, Germany

[‡]Deutsches Elektronensynchrotron DESY, Notkestr. 85, 22607 Hamburg, Germany

[§]Institute of Nanotechnology, Karlsruhe Institute of Technology (KIT), Hermann-von-Helmholtz-Platz 1, D-76344 Eggenstein-Leopoldshafen, Germany

Supporting Information

ABSTRACT: $Ba_{1-x}La_xF_{2+x}$ covering the whole range of compositions was synthesized by high-energy ball milling of mixtures of BaF_2 and LaF_3 at ambient temperature. The compounds obtained in this way crystallize in the cubic fluorite structure in the range from $0 \le x \lesssim 0.775$ which extends the range for the fluorite-type $Ba_{1-x}La_xF_{2+x}$ covered up to now ($0 \le x \le 0.55$) considerably. By employing ^{19}F NMR spectroscopy and X-ray (total) scattering, indications for a continuous change from the fluorite (BaF_2) to the tysonite structure (LaF_3) were found. The mechanosynthesized samples showed slightly higher fluoride ion conductivities for the samples with $x \le 0.40$ and clearly smaller conductivities in the case of the samples with $x \ge 0.85$ than reported for their monocrystalline counterparts. Two conductivity maxima at $x \approx 0.40$ and $x \approx 0.85$ and a conductivity minimum at $x \approx 0.75$ were observed for the mechanosynthesized $Ba_{1-x}La_xF_{2+x}$. For the samples with $0.10 \le x \le 0.50$, exhibiting a dc conductivity in the order of 10^{-5} S/cm at 400 K, all fluoride ions seem to be highly mobile at temperatures beyond 453 K. The decrease of the ionic conductivity observed for $Ba_{1-x}La_xF_{2+x}$ with increasing x in the range from $x \approx 0.50$ to $x \approx 0.75$ is accompanied by a change of the diffusion behavior and a decrease of the ratio of highly mobile to nonmobile or slow fluoride ions.

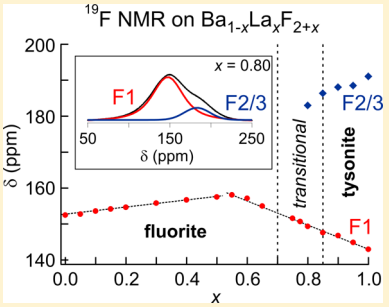

I. INTRODUCTION

Over the last years it has become apparent that compounds ground or synthesized by high-energy ball milling often show a change in their properties, e.g., an enhanced ionic conductivity, compared to their micro- or monocrystalline counterparts prepared by conventional solid state synthesis routines.[1−5] Furthermore, the synthesis of compounds conducted by mechanical treatment of the starting materials, the so-called mechanosynthesis, is known to be a very efficient technique for the preparation of metastable, partly new, compounds.[5−7] A well-known specialty of this technique is the preparation of solid solutions of normally immiscible or hardly miscible phases.[5−9] In this respect, the BaF_2−LaF_3 system is of particular interest. $Ba_{1-x}La_xF_{2+x}$ crystallizes in the fluorite structure (space group $Fm\bar{3}m$) for compositions $x \lesssim 0.55$[10,11] and in the tysonite structure (space group $P\bar{3}c1$) for $x \gtrsim 0.85$[10,11]. In the intermediate composition range from $x \approx 0.55$ to $x \approx 0.85$, the system is characterized by a miscibility gap.[10,11]

The microstructure, or more specifically the fluoride ion sublattice of fluorite-type $Ba_{1-x}La_xF_{2+x}$, turned out to be quite complex. By neutron scattering experiments some indications for the formation of so-called 2:2:2 clusters were found for the fluorite-type $Ba_{1-x}La_xF_{2+x}$ with $x \gtrsim 0.05$.[12,13] These 2:2:2 clusters consist of two fluoride ion interstitials ($x = 0.5$, $y = 0.32$, $z = 0.32$)[14] denoted as F′, two fluoride ion interstitials ($x = 0.46$, $y = 0.46$, $z = 0.46$)[14] denoted as F″ and two F^- vacancies ($x = 0.25$, $y = 0.25$, $z = 0.25$).[14] Chernov et al.[15] argued that the structure of these clusters resembles structural elements of the tysonite structure. This assumption was corroborated by results of Kadlec et al.[16] who found vibration modes in $Ba_{1-x}La_xF_{2+x}$ similar to those in LaF_3. Hence, an investigation of the transition of $Ba_{1-x}La_xF_{2+x}$ from the fluorite structure to the tysonite structure seems tempting. In addition, the 2:2:2 clusters are assumed to be responsible for the enhanced ionic conductivity observed for the compounds with $0.05 \lesssim x \lesssim 0.50$.[16−20] According to the enhanced ionic motion model,[18,21] the structural relaxation of the BaF_2 lattice close to the clusters leads to a decrease of the migration barriers of the fluoride ions. As a consequence, percolation paths for the fluoride ions should be formed in the interface regions of the moderate fluoride ion conductor BaF_2 and the presumed nonconducting 2:2:2 clusters.[18,21] It should be noted that in contradiction to the latter assumption, which is based on calculations regarding the stability of the 2:2:2 clusters,[18,22] the results of Andersen et al.[13] indicate that at least some of the fluoride ions in the 2:2:2 clusters are mobile.

Due to its high ionic conductivity $Ba_{1-x}La_xF_{2+x}$ was already used as a solid fluoride ion conductor in a chemical sensor[23]

Received: October 8, 2013
Revised: January 17, 2014

   dx.doi.org/10.1021/jp410018t | J. Phys. Chem. C XXXX, XXX, XXX−XXX

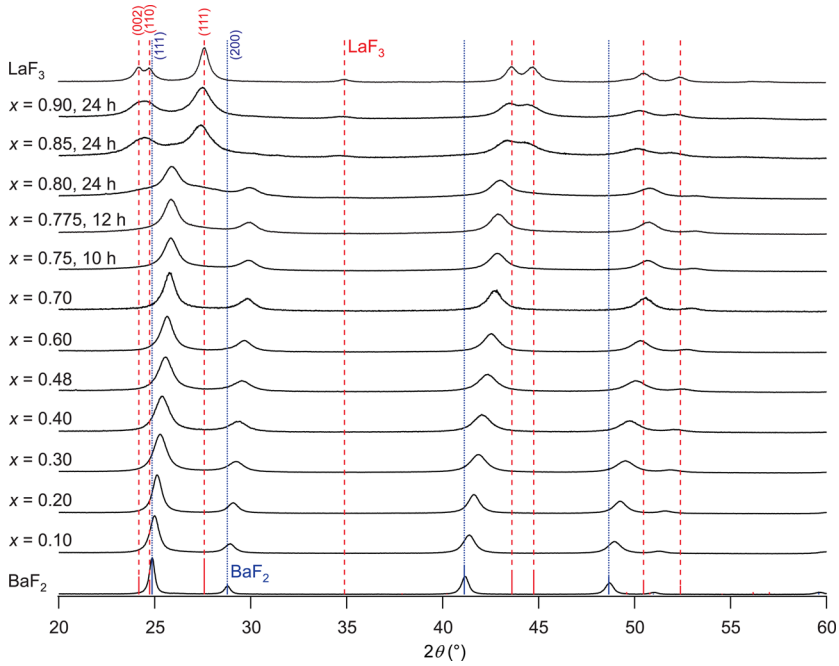

Figure 1. XRPD patterns of the different $Ba_{1-x}La_xF_{2+x}$ compounds. If not stated otherwise all compositions were milled for six hours. With a decreasing amount of BaF_2 (blue bars) the corresponding peaks shift to larger 2θ values in the case of the compounds which crystallize in the fluorite structure. For $x > 0.80$ the samples show the typical XRPD pattern of LaF_3 (red bars) shifted to smaller values of 2θ. See text for further explanations.

and as an electrolyte in a fluoride ion battery.[24] Fluoride ion batteries have found some attention in the past and present since they promise a large inherent safety and very high capacities.[23−34] For this kind of batteries, in which a reaction of the type $MF_y + M' \rightleftharpoons M + M'F_y$ (M = metal) takes place, only ceramic electrolytes have been tested, yet. Therefore, the fluoride ion battery systems exhibiting a high specific energy investigated up to now can only be operated at elevated temperatures due to the rather low ionic conductivity of the electrolytes being stable in a sufficiently broad potential range. The latter criterion most probably excludes the usage of the very fast known fluoride ion conductors containing lead or tin[35] like PbF_2,[36] $PbSnF_4$,[37] and presumably also $BaSnF_4$. Thus, other fast fluoride ion conductors have to be found. $Ba_{1-x}La_xF_{2+x}$ seems to offer a high electrochemical stability[38] but in comparison with, e.g., $PbSnF_4$ a rather low ionic conductivity.[20,37] As already mentioned, the ionic conductivity of several ceramic compounds could be increased by mechanical treatment or mechanosynthesis. Furthermore, as stated above, the miscibility gap of BaF_2 and LaF_3 may be closed by employing a mechanosynthesis routine.[6] Hence, mechanosynthesis may open up a path to the preparation of $Ba_{1-x}La_xF_{2+x}$ compounds which exhibit higher ion conductivities than observed so far for this system.

Therefore, in this study the ionic conductivity of mechanosynthesized $Ba_{1-x}La_xF_{2+x}$ with $0 \leq x \leq 1$ was investigated by impedance spectroscopy. Further insight regarding the fluoride ion diffusion in the prepared materials was gained by ^{19}F nuclear magnetic resonance (NMR) spectroscopy. The structure and microstructure of the samples were investigated by X-ray powder diffraction (XRPD), transmission electron microscopy (TEM), and ^{19}F magic angle spinning (MAS) NMR spectroscopy. For some samples X-ray scattering experiments were done up to large q-values to calculate their pair distribution functions (PDFs), $G(r)$.

II. EXPERIMENTAL DETAILS

A series of samples with compositions $Ba_{1-x}La_xF_{2+x}$ with $0 \leq x \leq 1$ were prepared by joint milling of micrometer-sized pure BaF_2 (99.99%, Sigma Aldrich) and LaF_3 (99.9%, Fluka). The synthesis was carried out using a Fritsch P7 premium line planetary mill employing a ZrO_2 milling vial set (45 mL) in combination with 140 milling balls (5 mm in diameter) of the same material. The total mass of each mixture was 2.0000(5) g. Milling times t_{mill} used reached from 6 to 24 h. The temperature of the milling beaker was measured with a pyrometer in the inside of the beaker directly after milling. It did not exceed 343 K.

The obtained powders were characterized by XRPD using a D8 Advance diffractometer (Bruker) operating with Cu−K_α radiation at 40 kV which corresponds to a wavelength $\lambda \approx 0.154$ nm. For some of the samples PDFs were calculated from X-ray diffractograms obtained at the High-Resolution Powder Diffraction (HRPD) beamline P02.1 of the PETRA III electron storage ring at DESY (Hamburg, Germany) in transmission mode. The energy of the synchrotron radiation was set to 59.81 keV, which corresponds to a wavelength of $\lambda = 0.02073$ nm. Two-dimensional XRD patterns were collected using a Perkin-Elmer 1621 fast image plate detector (2048 × 2048 pixels, 200 × 200 μm^2 pixel size) carefully mounted orthogonal to the X-ray beam. The samples were illuminated for 10 s by the X-ray beam. For each sample measurements were done with different distances between the sample and detector to obtain the best resolution in the low as well as the high q-range. The two-dimensional XRPD patterns were integrated to the q-space by employing the software package FIT2D.[39] This results in several one-dimensional XRPD patterns for different ranges of q which were merged to a single pattern for each sample. The obtained diffractograms were corrected (absorption, fluorescence, Compton scattering, etc.) and eventually Fourier transformed to PDFs by employing the software PDFgetX2.[40]

dx.doi.org/10.1021/jp410018t | J. Phys. Chem. C XXXX, XXX, XXX−XXX

For TEM investigations, the powdered sample was dispersed in isopropyl alcohol. A drop of approximately 10 μL of this suspension was dried on a copper-supported holey carbon film. (S)TEM was done at 200 kV on a field-emission instrument of the type JEOL JEM-2100F-UHR.

The impedance measurements were done on cylindrical pellets with a diameter of 8 mm and approximately 1 mm thickness (measured with a vernier caliper for each pellet). The pellets were produced by cold-pressing the powders at a uniaxial pressure of about 1 GPa. Electrodes were applied by coating the plane parallel sides of the pellets with an alcohol-based graphite conductive adhesive (Alfa Aesar). The measurements were done with an HP 4192 A analyzer connected to a home-built cell with a four-terminal configuration in the frequency range from 5 Hz to 13 MHz. The cell is designed to be operated under controlled atmospheres. Here, a constant flow of dry argon gas (99.999%) was applied. A Eurotherm controller was used to monitor and adjust the temperature.

For the temperature-variable static ^{19}F NMR measurements the powdered samples were put into glass ampullae, dried in vacuum at 380 K for at least 24 h, and then heat sealed. The measurements were done with an MSL 400 spectrometer (Bruker) connected to a shimmed Oxford cryomagnet with a nominal field of 9.4 T which corresponds to an ^{19}F resonance frequency of ν_0 = 376.5 MHz. A modified 7 mm MAS NMR probe (Bruker Biospin) was used for the measurements. The duration of the $\pi/2$ excitation pulse applied was 3.3 μs. For all measurements the saturation recovery pulse sequence was used, followed by an adjustable waiting time and a single $\pi/2$ pulse.[41,42] For each spectrum 32 scans were accumulated. To obtain fully relaxed spectra the waiting time was chosen to be five times the relaxation time T_1 at the respective temperature.

The ^{19}F MAS NMR spectra were recorded with an Avance III spectrometer (Bruker) operating at ν_0 = 564.7 MHz by employing a 1.3 mm MAS probe (Bruker) and using room-temperature bearing gas. The NMR spectra were acquired by applying a single $\pi/2$ excitation pulse with a length of approximately 2 μs. For each spectrum 32 scans were accumulated with a recycle delay of 5 s and a spinning speed of ν_{rot} = 60 kHz. All ^{19}F NMR spectra were referenced to C_6F_6 (which has a chemical shift δ = −162.9 ppm when referenced to CCl_3F[43]).

III. RESULTS AND DISCUSSION

A. Characterization by X-ray Diffraction. Starting from pure BaF_2 all XRPD peaks of the $Ba_{1-x}La_xF_{2+x}$ show the typical pattern of the fluorite structure in a range from $0 \le x \le 0.775$ (see Figure 1). The positions of the peaks are shifted toward larger 2θ values with increasing amounts of LaF_3 which indicates lattice contraction. Even the sample with x = 0.80 shows the typical pattern of the fluorite structure, but there are also some very broad peaks of weak intensity exhibiting the XRPD pattern (particularly the (002), (110), and (111) peaks) of LaF_3 crystallizing in the tysonite structure which seem to be shifted toward smaller values of 2θ. It should be noted that an increase of the milling time from 24 to 60 h or the change of the milling vial set does not lead to the disappearance of the XRPD peaks of the tysonite phase in the case of the sample with x = 0.80 (see Figure S1, Supporting Information). In the case of the sample with x = 0.85, the shifted (111) and (200) peaks of the BaF_2 pattern can still be detected at approximately 26° 2θ and 30.1° 2θ besides the typical pattern of LaF_3 (space group $P\bar{3}c1$) shifted toward smaller values of 2θ. Thus, these two samples seem to be mixtures of $Ba_{1-x}La_xF_{2+x}$ crystallites of which a part crystallizes in the fluorite and the other ones in the tysonite structure. The width of the small peaks in the case of the sample with x = 0.80 makes a clear assignment to a phase difficult. Thus, judging from the XRPD pattern it cannot be excluded that just residual pure LaF_3 or amorphous material is present. However, it should be noted that both structures should be highly distorted in this range of compositions as will be discussed later. Thus, one might assume that the samples with x = 0.80 and x = 0.85 may be transitional phases combining structural aspects of both structures and are not mixtures of differently structured crystallites of $Ba_{1-x}La_xF_{2+x}$, which is essentially in agreement with the deliberations of Chernov et al.[15] (vide supra). The samples with x > 0.85 show the XRPD pattern of LaF_3 in which the peaks are shifted toward smaller diffraction angles which indicates lattice expansion.

The PDFs, i.e., G as a function of r, of the samples with x = 0.20, x = 0.50, x = 0.70, x = 0.80, and x = 0.85, shown in Figure 2, exhibit the average distances r of the ions in real space or, to

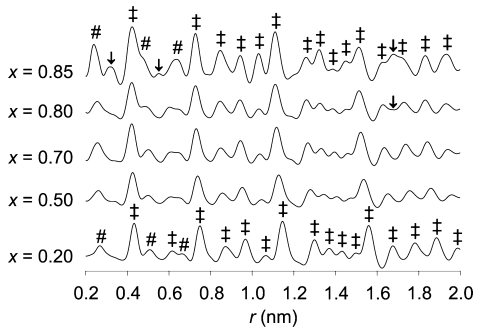

Figure 2. Pair distribution functions of several $Ba_{1-x}La_xF_{2+x}$ compounds. ‡ marks M−M distances, while # shows the distances between M and F. See text for further explanations.

be more exact, the probability to find ions in a certain distance from each other (by integration of $G(r)$ from r_1 to r_2).[44] At first view the patterns of all the samples are very similar. Even in the case of the sample with x = 0.85 exhibiting an XRPD pattern typical of the tysonite structure (see Figure 1), almost all of the peaks visible in the PDFs of the other samples crystallizing in the fluorite structure still show up. Starting from the sample with x = 0.20 the distances between the ions decrease with increasing x as was already observed in the XRPD patterns in Figure 1. The lattice parameters a of the fluorite type $Ba_{1-x}La_xF_{2+x}$ can easily be recognized in the PDFs of the samples as the second from left of the M−M (M = Ba^{2+}, La^{3+}) peaks, which are marked with an ‡. They are in good agreement with the ones obtained directly from the XRPD patterns (vide infra).

Going from x = 0.80 to x = 0.85 the change of the structures can be observed by the disappearance of the peak representing the lattice parameter a of the fluorite lattice, the emergence of three new peaks (arrows in Figure 2), and a change of the height of some of the peaks already present in the PDFs of the other samples. Furthermore, the first peak is clearly shifted to smaller r (0.24 nm) and shows a higher intensity compared to the peak representing the shortest M−F distance in the case of the sample with x = 0.80. It can be attributed to the shortest distance between La^{3+} and F^- in the tysonite structure. The new peak at 0.32 nm probably represents a cation−fluoride ion

dx.doi.org/10.1021/jp410018t | J. Phys. Chem. C XXXX, XXX, XXX−XXX

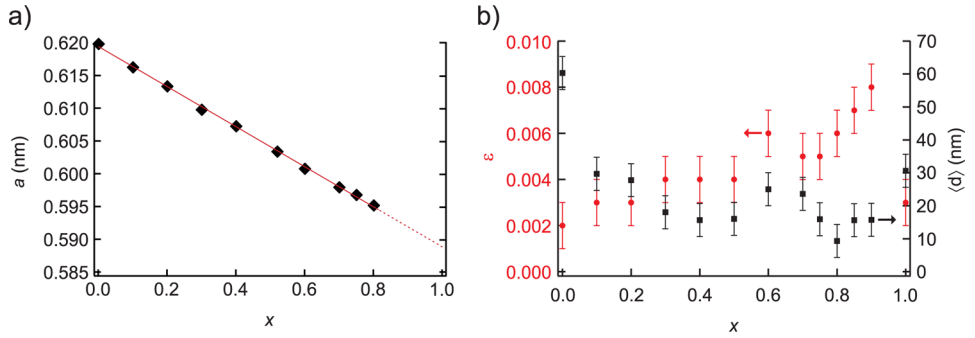

Figure 3. (a) Lattice parameter a of the $Ba_{1-x}La_xF_{2+x}$ compounds exhibiting the fluorite structure, whose XRPD patterns are shown in Figure 1, as a function of composition x. (b) Average crystallite size $\langle d \rangle$ (black squares) and lattice strain ε (red circles) as a function of x.

distance in the tysonite structure since it is too small for a cation−cation distance. Thus, this peak is probably associated with a Ba−F distance in the tysonite structure. The other new peak at 0.55 nm probably shows a Ba−Ba distance of Ba ions neighboring each other in the tysonite structure. This assumption is in good agreement with the assumed Ba−F distance of about 0.32 nm and the low intensity of the peak, representing the expected low abundance of this pair. The last new peak in the shown distance regime at 1.68 nm can probably be attributed to a La−La distance in the tysonite structure. A similarly positioned peak seems to exist also in the sample with $x = 0.80$ (marked by an arrow). Apart from these three peaks, the La−F peak at 0.24 nm, and several changes in the intensity of some of the cation−cation peaks due to different coordination numbers, the PDF of the tysonite structured $Ba_{0.15}La_{0.85}F_{2.85}$ is similar to the ones of the fluorite structured samples.

There are no peaks in the PDFs which can clearly be associated with the M−F distances in the 2:2:2 clusters (the M−M distances are the same as in the undistorted fluorite structure). These distances are, however, rather close to the ones in the undistorted fluorite structure and, therefore, difficult to separate from each other. However, there should be a peak between the first two peaks in the PDFs of the samples with $x = 0.20$ up to $x = 0.80$ corresponding to the distances between the cations and the fluoride ions at F′ and F″ sites. In fact, a broad shoulder can be seen in this range in the case of the samples with $x = 0.20$, $x = 0.50$, and $x = 0.80$ but not for the sample with $x = 0.70$. Whereas the sample with $x = 0.70$ lacks such a shoulder, its first M−F peak is clearly broader and larger than observed for the other samples. Thus, one might assume a change of the cluster structure for this sample. Furthermore, it should be noted that the position of the second smallest d(M−F) peak changed in a pronounced way: from about $r = 0.50$ nm in the case of the sample with $x = 0.70$ to $r = 0.48$ nm for the sample with $x = 0.80$. Therefore, the shoulder in the case of the sample with $x = 0.80$ is probably not due to the 2:2:2 clusters but may rather be related with the peak at 0.32 nm appearing in the PDF of the sample with $x = 0.85$ which probably represents the shortest Ba−F distance in the tysonite structure (vide supra).

Although the PDFs of the samples with $x = 0.80$ and $x = 0.85$ seem to be quite similar, the PDF of the sample with $x = 0.80$ is still more similar to the PDFs of the samples with $x = 0.20$, $x = 0.50$, and $x = 0.70$. Coming back to the question regarding the actual structure of the sample with $x = 0.80$, it can be seen that the PDF of this sample indeed combines aspects of the PDFs of the samples with $x = 0.70$ and $x = 0.85$ without showing identical peaks. There are also no peaks in the PDF of the sample with $x = 0.80$ which can clearly be matched with distances in pure LaF_3 (which admittedly does not rule out the possibility of the presence of a small amount of LaF_3 in this sample). Therefore, it seems reasonable to assume that the sample with $x = 0.80$ is not a mixture of $Ba_{1-x}La_xF_{2+x}$ crystallizing in the fluorite and $Ba_{1-x}La_xF_{2+x}$ crystallizing in the tysonite structure. Instead of this, it seems to crystallize in a structure in between these structures.

In Figure 3a the lattice parameter a of the $Ba_{1-x}La_xF_{2+x}$ crystallizing in the (structurally distorted) cubic fluorite structure, calculated according to

$$a = \frac{\lambda_{XRD}}{2 \cdot \sin \theta} \cdot \sqrt{(h^2 + k^2 + l^2)} \quad (1)$$

is shown as a function of x. Here $\lambda_{XRD} = 0.154$ nm is the average wavelength of the X-ray radiation used, and h, k, and l are the Miller indices of BaF_2. The positions of the maxima of the first ten peaks were used for the calculations. With increasing amount of LaF_3 the lattice parameters a of the compounds decrease linearly in the range $0 \leq x \leq 0.80$. The slope of the line is 0.0306(4) and, thus, very similar to the one reported by Sobolev et al. for monocrystalline $Ba_{1-x}La_xF_{2+x}$[11] which is 0.03033. This indicates that the intended amounts of LaF_3 were introduced into the BaF_2 lattice for $x \leq 0.80$.

The XRPD peaks of the $Ba_{1-x}La_xF_{2+x}$ are very broad. This can inter alia be caused by a reduced number of scattering centers (atomic planes) due to size reduction of the crystallites or by lattice strain which leads to a distribution of distances between the atomic planes. Interestingly, the peaks of the binary fluorides are less broad than the ones of the $Ba_{1-x}La_xF_{2+x}$ products. This is probably mainly due to an enhanced size reduction caused by the mechanical interaction of the $Ba_{1-x}La_xF_{2+x}$ crystallites with each other or with the starting materials which seems to be more effective than in the case of the pure binary fluorides.

This is indicated by the results obtained by employing the procedure introduced by Williamson and Hall[45] using the full width at half-maximum (fwhm) of the XRPD peaks corrected for instrumental broadening effects (see ref 4 for more details). Values of the average crystallite size $\langle d \rangle$ in a range from 9(5) nm ($x = 0.80$) to 29(5) nm ($x = 0.10$) were found for $Ba_{1-x}La_xF_{2+x}$ without a continuous trend when plotted as a function of x (see Figure 3b). The lattice strain ε varies from 0.002(1) to 0.008(1) and increases with x (Figure 3b) which indicates increasing structural disorder with rising x. In the case of the ball-milled binary fluoride, values of 60(5) nm ($\varepsilon = 0.002$) for BaF_2 and 31(5) nm ($\varepsilon = 0.003$) for LaF_3 were

dx.doi.org/10.1021/jp410018t | J. Phys. Chem. C XXXX, XXX, XXX−XXX

determined. The average crystallite size can also be estimated from the PDFs as the distance r at which $G(r)$ cannot be separated from noise anymore (see Figure S2, Supporting Information). The values obtained that way are in quite good agreement with the values obtained by the Williamson and Hall approach.

In Figure 4 a high-resolution (HR)TEM micrograph of the sample with $x = 0.80$ is shown. The crystallites were found in

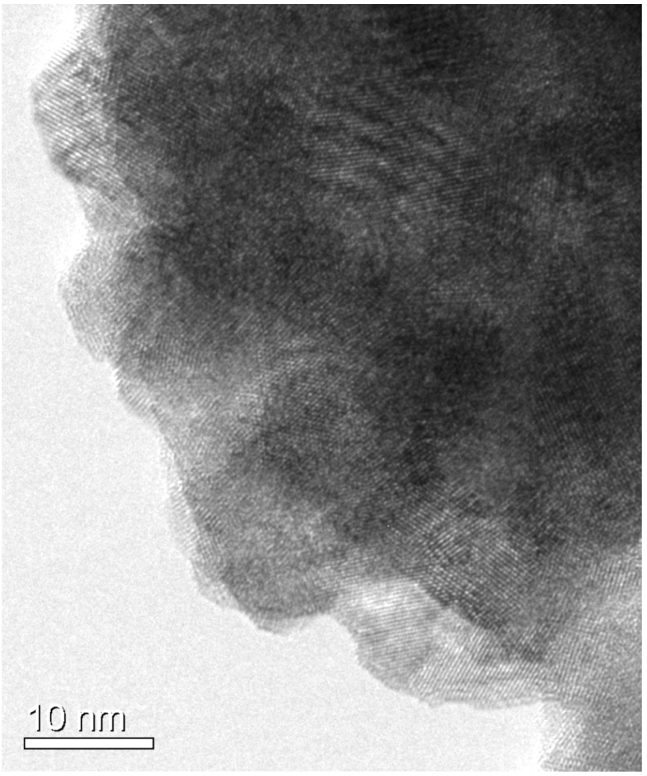

Figure 4. HRTEM micrograph of the sample with $x = 0.80$.

agglomerates and exhibit diameters of approximately 10 nm which is in good agreement with the value calculated from the XRPD and the PDF. They show a well-ordered structure even at their boundaries.

The thermal stability of $Ba_{1-x}La_xF_{2+x}$ was tested for the samples with $x = 0.80$ and $x = 0.65$. After heat treatment for 6 h at 873 K in air the XRPD patterns exhibit the formation of LaF_3 besides $Ba_{1-x}La_xF_{2+x}$ (see Figure 5). The XRPD peaks of the $Ba_{1-x}La_xF_{2+x}$ are narrowed which is due to grain growth or decreased lattice strain, and they are shifted to smaller values of 2θ. Thus, the $Ba_{1-x}La_xF_{2+x}$ compounds were depleted in LaF_3 by thermal treatment. Several additional peaks of weak intensity are also visible which we were not able to attribute to a known phase. Since the lattice parameter a of the $Ba_{1-x}La_xF_{2+x}$ crystallizing in the fluorite structure changes linearly with x it was possible to calculate the compositions of the annealed samples. They changed from $x = 0.80$ to $x = 0.66$ and from $x = 0.65$ to $x = 0.57$, respectively. Thus, the higher the LaF_3 content of the thermally treated $Ba_{1-x}La_xF_{2+x}$, the more pronounced is the depletion of LaF_3. Hence, as already expected, the fluorite-type $Ba_{1-x}La_xF_{2+x}$ with $0.55 \lesssim x \lesssim 0.80$ is metastable at room temperature and most probably cannot be prepared by conventional solid state synthesis.

B. ^{19}F MAS NMR Spectroscopy. For several mixed fluoridic systems it was possible to receive an impression of the unequal cationic environments of the fluoride ions and, thus, of the microstructure of the materials by ^{19}F MAS NMR spectroscopy using high spinning speeds.[6,7,46] However, the spectra obtained for the $Ba_{1-x}La_xF_{2+x}$ do not allow a separation of the different cationic environments of the fluoride ions (see Figure 6). Whereas in the case of solid solutions of BaF_2 and CaF_2[6], BaF_2 and SrF_2,[6] or CaF_2 and SrF_2,[6,46] which crystallize in the fluorite structure, up to five NMR lines, representing the five possible cationic environments of the tetrahedrally coordinated fluoride ions, were observed, here at maximum two NMR lines can be separated (see Figure 6). This is due to several characteristics of this system. First, the isotropic chemical shifts δ_{iso} of the ^{19}F NMR lines of BaF_2 (152 ppm) and LaF_3 (143 and 192 ppm) are close to each other. Furthermore, the mechanical treatment of the pure binary fluorides leads to a broadening of their NMR lines (see Figure 6). The high defect concentration in the mechanically treated materials, especially in the grain boundary affected regions of the crystallites, leads to a large amount of fluoride ions situated in slightly different chemical environments. Hence, these fluoride ions experience slightly different magnetic field strengths leading to a manifold of NMR lines with similar chemical shifts which merge into a broad NMR line. This line broadening eases the superposition of NMR lines which are separated in the case of well-ordered materials. However, the presumably most important aspect is the fact that the excess positive charge of the La ions substituting the Ba ions in the BaF_2 has to be compensated by fluoride ions sitting on interstitial sites which leads to the formation of a structurally distorted lattice. For instance, in the case of $Ba_{0.5}La_{0.5}F_{2.5}$ in theory 1/5 of the fluoride ions have to occupy interstitial sites. As already mentioned before, indications for the formation of 2:2:2 clusters, hosting the additional fluoride ions in monocrystalline $Ba_{1-x}La_xF_{2+x}$, were found by neutron scattering.[13] Since the slope of the lattice parameter as a function of x is very similar to the one found for single crystals and judging from the PDFs (vide supra), it seems likely that also for the mechanosynthesized $Ba_{1-x}La_xF_{2+x}$ these (or similar) cluster structures are formed at least for the samples with $x < 0.70$. Especially in the case of large x many fluoride ions should be situated in slightly different chemical environments, e.g., fluoride ions at the different sites in the 2:2:2 clusters, fluoride ions on regular sites close to displaced fluoride ion sites, fluoride ions coordinated by different cation species, or fluoride ions experiencing strain in the fluorite structure for instance close to the 2:2:2 clusters. Thus, there should be many NMR lines with slightly different chemical shifts which apparently cannot be resolved anymore. As a consequence very broad NMR lines emerge.

The fluoride ions at some of the sites associated with the 2:2:2 clusters might be represented by the NMR line with an isotropic chemical shift of about 170 ppm in the spectrum of the sample with $x = 0.05$ (see Figure 6), which was also reported by Rongeat et al.[47] This NMR line increases in intensity with increasing x and, thus, increasing amount of excess fluoride ions until it overlaps with the central NMR line. That way an increasingly broad NMR line with a fwhm of up to 57 ppm for the sample with $x = 0.775$ is obtained. Thus, when sticking to this hypothesis the 2:2:2 clusters and the fluorite-type structure cannot be distinguished in the case of $Ba_{1-x}La_xF_{2+x}$ with $x > 0.40$ which implies that the whole material is strongly affected by the 2:2:2 clusters in that compositional range.

dx.doi.org/10.1021/jp410018t | J. Phys. Chem. C XXXX, XXX, XXX−XXX

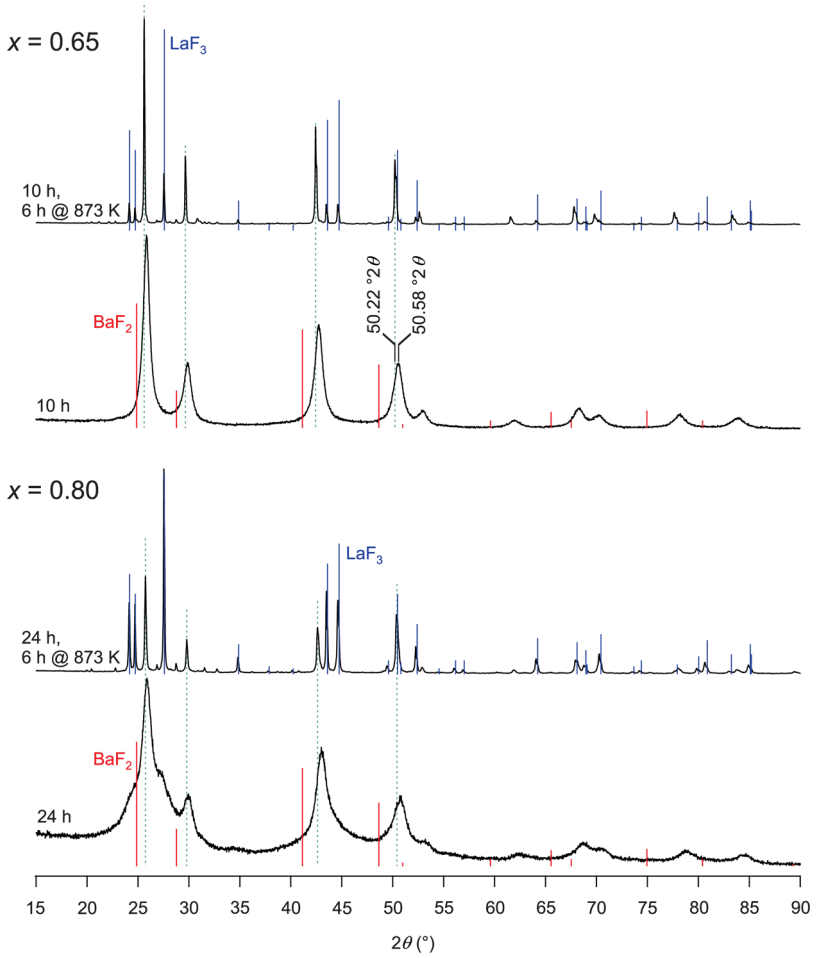

Figure 5. XRPD patterns of $Ba_{0.35}La_{0.65}F_{2.65}$ (top) and $Ba_{0.20}La_{0.80}F_{2.80}$ (bottom) after annealing for 6 h at 873 K in comparison to the XRPD patterns of the mechanosynthesized samples with the milling times 10 and 24 h, respectively, before annealing. The green dotted lines show the positions of the XRPD peaks of the $Ba_{1-x}La_xF_{2+x}$ after annealing. The red bars indicate the positions of the XRPD peaks of BaF_2 and the blue bars the ones of LaF_3.

In the spectra of milled BaF_2 and of the sample with $x = 0.05$ also the NMR lines representing orthorhombic BaF_2[3] (black arrows in Figure 6) can be found. Orthorhombic BaF_2 is a high-pressure phase of BaF_2[48,49] and known to form while milling.[3,7,48] For LaF_3, which crystallizes in the tysonite structure, three NMR lines in the case of monocrystalline material were observed.[50] These three NMR lines can be attributed to the three different sites of the fluoride ions, F1, F2, and F3, in the LaF_3 lattice (see ref 50). The fluoride ions on the F1 sites exhibit a chemical shift of approximately 143 ppm, while the ones on F2 and F3 sites (which do not differ that much from each other regarding their local cationic environments) can be found at around 192 ppm (see Figure 6). The fluoride ions on the F1 sites are coordinated by 4 La^{3+} which differ in distance d(La−F): 0.246, 0.248, 0.264, and 0.300 nm.[51] The fluoride ions on the F2 and F3 sites are coordinated by 3 La^{3+} with a distance d(La−F) of approximately 0.242 and 0.244 nm, respectively.[51] These short distances lead to the large chemical shifts observed compared to the one representing the fluoride ions on the F1 sites with clearly larger cation−fluoride ion distances.[52]

The NMR lines representing the fluoride ions on the F2 and F3 sites cannot be separated in the ^{19}F MAS NMR spectra of high-energy ball-milled LaF_3. With decreasing x the two NMR lines representing the fluoride ions on F1 sites or fluoride ion sites in the structurally distorted fluorite lattice and the fluoride ions on F2/3 sites converge until for the sample with $x = 0.75$ the two NMR lines can hardly be separated and eventually for the sample with $x = 0.65$ only a single NMR line is observed. Thus, with decreasing x the chemical environments of the fluoride ions on the F2 and F3 sites become more and more similar to the ones of the fluoride ions on the F1 sites or the ones located in the fluorite-type $Ba_{1-x}La_xF_{2+x}$. Hence, the microstructure seems to become more homogeneous. Furthermore, this means that for the sample with $x = 0.75$ clearly and solely showing the XRPD pattern of the fluorite structure an NMR line of considerable intensity representing fluoride ions in distorted F2/3 sites can be seen (see the two fit-lines in the spectra in Figure 6), which is in agreement with the deliberations of Chernov et al.[15] and the results of Kadlec et al.[16] (see Section I). It should be kept in mind that the TEM micrographs as well as the XRPD patterns show no hints for noteworthy amounts of amorphous material. Hence, it seems that the structure of the crystalline material is homogenized regarding the fluoride ion coordination spheres. These results indicate a continuous transition from the fluorite to the tysonite structure.

As observed for the lattice parameter (see Figure 3a), also in the case of the chemical shift a linear dependence on x is observed as shown in Figure 7. The change of the chemical shift

dx.doi.org/10.1021/jp410018t | J. Phys. Chem. C XXXX, XXX, XXX−XXX

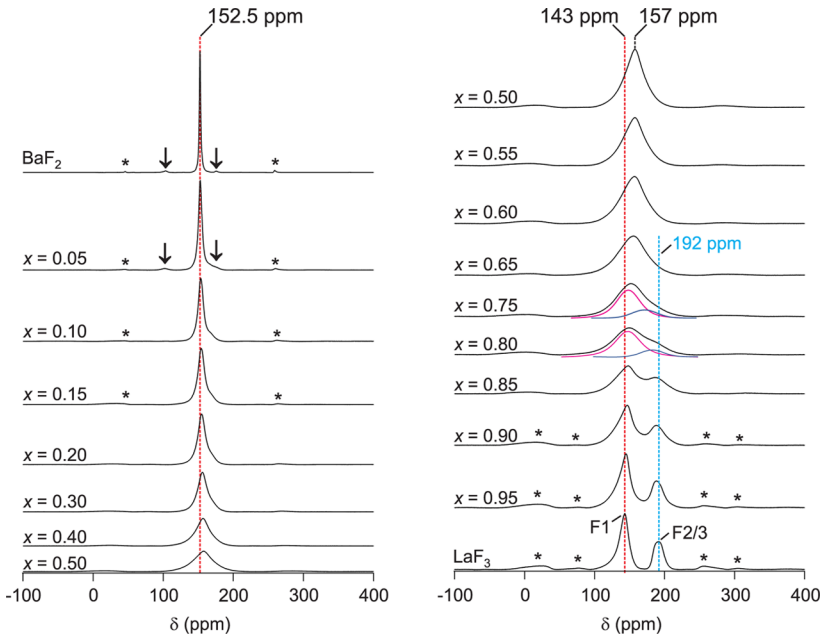

Figure 6. ^{19}F MAS NMR spectra of $Ba_{1-x}La_xF_{2+x}$ with the compositions x as indicated, recorded at ν_0 = 565 MHz with ν_{rot} = 60 kHz. For comparison also the spectra of the milled binary fluorides are shown. The spectra of the samples with x = 0.75 and x = 0.80 were fitted by two lines (see text for further explanations). The arrows show the NMR lines representing orthorhombic BaF_2. Spinning sidebands are marked by asterisks.

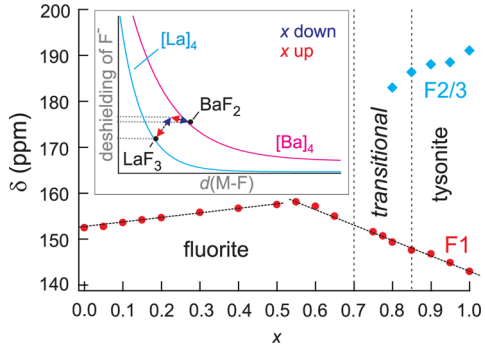

Figure 7. Variation of the chemical shift of ^{19}F in $Ba_{1-x}La_xF_{2+x}$ with x. The red points denote the maxima of the main NMR lines in Figure 6 corresponding to F^- on their sites in the fluorite structure and F1 sites in the tysonite structure. The blue rhombi denote the maxima of the less intense NMR lines clearly visible for the samples with $x \geq 0.80$ corresponding to F^- on F2 and F3 sites in the tysonite structure. The inset shows the deshielding of the F1 fluoride ions and the ones in the fluorite structure by the two cation species as a function of the distance between cation and fluoride ion d(M−F). See text for further explanations.

is associated with d(M−F), as was already discussed in refs 6 and 7. However, the NMR line representing the fluoride ions on the F1 sites shifts toward larger chemical shift values with increasing amounts of BaF_2 and, thus, increasing lattice parameter. At first glance this seems unexpected since an expanding lattice, and thus expanding distances d(La/Ba−F), should lead to a decrease of the isotropic ^{19}F NMR chemical shift.[6,7,52] In fact such a behavior can be seen for the NMR line representing the fluoride ions on F2/3 sites (see Figure 7). Therefore, the increase of the chemical shift is most probably due to a larger deshielding of the fluoride ions by the Ba ions introduced with respect to the La ions. Simply put, the value of the isotropic ^{19}F NMR chemical shift can be treated as the sum of the diamagnetic shielding and the paramagnetic deshielding of the fluoride ions. The diamagnetic shielding is caused by the electrons of the fluoride ion and is not affected by its chemical environment. The paramagnetic deshielding, however, is caused by the electrons of the atoms or ions surrounding the fluoride ion. Its value can be determined by simply summing up the respective contributions of these atoms or ions.[52,53] Of course the separation of the diamagnetic shielding from the paramagnetic deshielding is rather hypothetical. The paramagnetic deshielding of the fluoride ion strongly depends on the distance d(M−F) in an exponential way.[52] Thus, the smaller the initial distance between the cation and the fluoride ion the larger the change of the isotropic chemical shift when d(M−F) is varied. Therefore, the fluoride ions on F2 sites can be distinguished from the fluoride ions at the almost identical F3 sites in polycrystalline LaF_3[50] despite that $\Delta(d(\text{M}-\text{F})) = d(\text{M}-\text{F3}) - d(\text{M}-\text{F2}) = 0.002$ nm. In BaF_2 a distance of 0.268 nm between the fluoride ion and the four Ba^{2+} leads to a chemical shift of 152 ppm. Although the distances d(La−F) of three of the four cations coordinating the fluorine on the F1 site in LaF_3 are clearly smaller than 0.268 nm, its chemical shift is only 143 ppm. Therefore, as may already be estimated from their different ionic radii, the deshielding of the La ions is smaller for this distance regime than the one of the Ba ions. Thus, the increase of the distances between the ions which should lead to a decrease of the chemical shift is overcompensated by the deshielding of the fluoride ions by the Ba ions. This leads to an increase of the isotropic chemical shift with decreasing x. However, when x is decreased below a certain value the expansion of the lattice should overcompensate the higher deshielding of the Ba ions due to the exponential decline of the deshielding with increasing d(M−F), as illustrated in the inset of Figure 7. Hence, the chemical shift should not increase anymore but start to decrease toward the chemical shift value of BaF_2. In fact, this is observed: starting at a composition of x = 0.55 the chemical shift value decreases with decreasing x (Figure 7).

dx.doi.org/10.1021/jp410018t | J. Phys. Chem. C XXXX, XXX, XXX−XXX

The decrease of the chemical shift of the NMR line representing the fluoride ions on the F2/3 sites with increasing BaF_2 content is also due to the substitution of the La ions coordinating these fluoride ions by Ba ions since the fluoride ions on F1 sites share their cationic neighbors with the fluoride ions on F2 and F3 sites. The increase of the, in this case initially very small, cation−fluoride ion distances (vide supra) causes a decrease of the chemical shift. This eventually leads to an averaging of the distances between fluoride ions and cations in the three coordinations spheres of the fluoride ions as already described before.

Interestingly, the change of the chemical shift with x in a range from $x = 0.55$ to $x = 1$ seems to be linear although in this range the macroscopic structure of $Ba_{1-x}La_xF_{2+x}$ changes from fluorite to tysonite. This means that the change of the chemical environment of the fluoride ions situated in $Ba_{1-x}La_xF_{2+x}$ crystallizing in the structurally distorted fluorite lattice to the one of the F1 sites in the $Ba_{1-x}La_xF_{2+x}$ crystallizing in the distorted tysonite structure is continuous.

It should be noted that the ^{19}F MAS NMR spectra of annealed samples (18 h at 823 K) of the stable compounds ($x \leq 0.55$), which are not shown here, do not differ in chemical shift or shape when compared with their mechanosynthesized counterparts but show just a slight decrease of the fwhm. Thus, the microstructure of the mechanosynthesized, nanocrystalline $Ba_{1-x}La_xF_{2+x}$ with $x \leq 0.55$ seems to be similar to the one of the microcrystalline $Ba_{1-x}La_xF_{2+x}$.

C. Ionic Conductivity of the Compounds. In Figure 8 the temperature dependence of the dc conductivity taken from

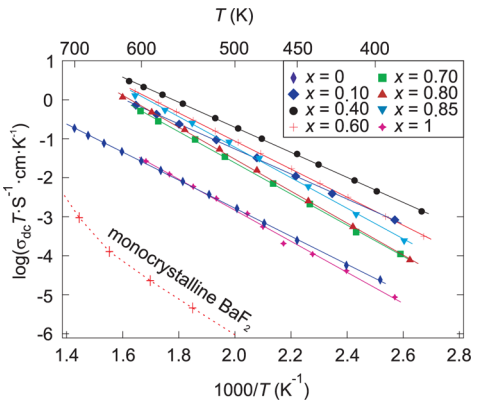

Figure 8. Logarithmic plot of the dc conductivities of some of the mechanosynthesized $Ba_{1-x}La_xF_{2+x}$ samples as a function of inverse temperature fitted by using the Arrhenius eq 2. For comparison also the dc conductivities of a BaF_2 single crystal taken from ref 19 are shown.

the frequency-independent plateaus of the conductivity spectra (σ as a function of frequency) of a selection of samples is shown in an Arrhenius representation according to

$$\sigma_{dc}T = A_0 e^{-E_a/(k_B T)} \quad (2)$$

with

$$A_0 = \frac{Nq^2fb^2}{H_r k_B 6\tau_0} \quad (3)$$

$$\tau_0^{-1} = \tau^{-1} e^{E_a/(k_B T)} \quad (4)$$

where E_a denotes the activation energy; N is the particle density of the charge carriers; b is the average jump distance of the mobile ions; q is the electric charge of the mobile ions; $0 \leq f \leq 1$ gives the degree of correlation of the ion jumps ($f = 1$: uncorrelated jumps); H_r is the Haven ratio; τ^{-1} is the average jump rate of the mobile ion; τ_0 is the pre-exponential factor; and k_B is Boltzmann's constant (see, e.g., ref 54). The milling times are the same as shown in Figure 1.

The ionic conductivities of the $Ba_{1-x}La_xF_{2+x}$ compounds are clearly larger than the ones found for the binary fluorides. Compared to the dc conductivity of monocrystalline BaF_2 reported by Sorokin et al.[19] the dc conductivity of the BaF_2 was also increased by approximately 3 orders of magnitude by high-energy ball milling (see also Figure 9a and refs 3 and 55). Interestingly, in the case of the LaF_3 the mechanical treatment shows no effect on the dc conductivity as can be seen by comparison with the ionic conductivity of a single crystal investigated by Sinitsyn et al.[56]

If the negative imaginary part of the impedance ($-Z''$) is plotted versus its real part (Z'), a single depressed semicircle is observed for all samples investigated in this study (see Figure S3, Supporting Information). Therefore, the conductivity in the grains cannot be distinguished from the one in the grain boundaries which makes an elucidation of the processes leading to the dc conductivities measured difficult.

The dc conductivity of the $Ba_{1-x}La_xF_{2+x}$ compounds varies with x in a range of approximately 0.6 orders of magnitude at a temperature of 588 K as shown in Figure 9a. Starting from pure ball-milled BaF_2 the conductivity increases by about 1 order of magnitude when going to $Ba_{0.90}La_{0.10}F_{2.1}$. A maximum of conductivity is observed for the sample with $x = 0.40$ which is in good agreement with the results of Rongeat et al.[47] for mechanosynthesized $Ba_{1-x}La_xF_{2+x}$ with $x \leq 0.55$. From $x = 0.40$ on, the dc conductivity decreases with increasing x until a minimum of the dc conductivity for the sample with $x = 0.75$ is reached. If x is increased further a second maximum occurs at $x = 0.85$. This behavior can be observed in a range from 350 to 588 K, although the positions of the maxima change from $x = 0.30$ and $x = 0.90$ at 350 K to $x = 0.40$ and $x = 0.85$ at 588 K, respectively (see Figure 9a).

In the range from $x = 0.10$ to $x = 0.40$ the dc conductivities at 588 K of the samples prepared are approximately 0.5 orders of magnitude larger than the ones reported for monocrystalline $Ba_{1-x}La_xF_{2+x}$ by Sorokin et al.[19] In the case of the sample with $x = 0.50$ the conductivities of the mechanosynthesized and the monocrystalline material are very similar (see Figure 9a). Sorokin et al.[19] as well as Wapenaar et al.[18] reported increasing conductivities and decreasing activation energies with increasing LaF_3 content from $x = 0$ to $x = 0.50$. Andersen et al., however, found no decrease of the activation energy going from $x = 0.209$ to $x = 0.492$ but a slight increase from 0.54 to 0.57 eV.[13] In the case of the $Ba_{1-x}La_xF_{2+x}$ samples prepared here the conductivities increase from $x = 0$ to $x = 0.40$, and the activation energies decrease between $x = 0$ and $x = 0.20$. However, it should be noted that the latter vary by only 0.05 eV in the range from $x = 0.10$ to $x = 0.50$ (see Figure 9b).

In Figure 9b also the pre-exponential factors A_0 of the mechanosynthesized samples are shown as a function of x. It can be seen that the pre-exponential factors of the binary fluorides are clearly smaller than the ones found for $Ba_{1-x}La_xF_{2+x}$. Interestingly, A_0 increases almost linearly from $x = 0.10$ to $x = 0.80$ where a maximum of A_0 is reached (see Figure 9b). Since A_0 depends on several parameters (cf. eq 3),

dx.doi.org/10.1021/jp410018t | J. Phys. Chem. C XXXX, XXX, XXX−XXX

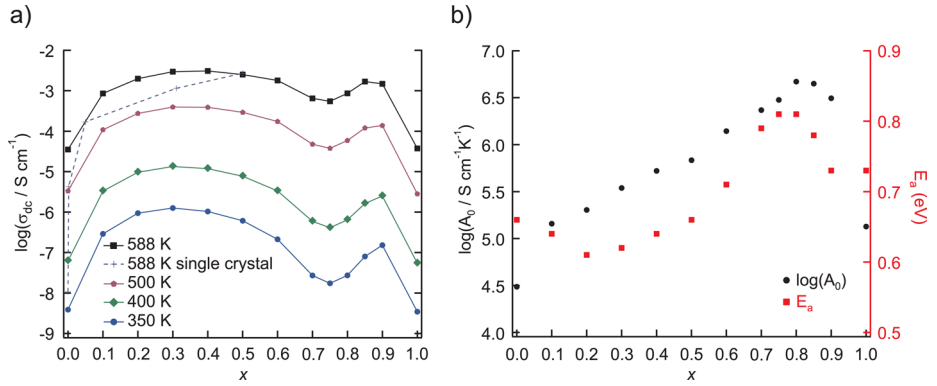

Figure 9. (a) Isothermes of the dc conductivities of mechanosynthesized $Ba_{1-x}La_xF_{2+x}$ as a function of x at the temperatures indicated. The lines are meant to guide the eye. For comparison also the isotherm of the dc conductivity of monocrystalline $Ba_{1-x}La_xF_{2+x}$ at 588 K taken from ref 19 is shown (dotted line). (b) Activation energies E_a and pre-exponential factors A_0 of the samples as a function of x. See text for further explanations.

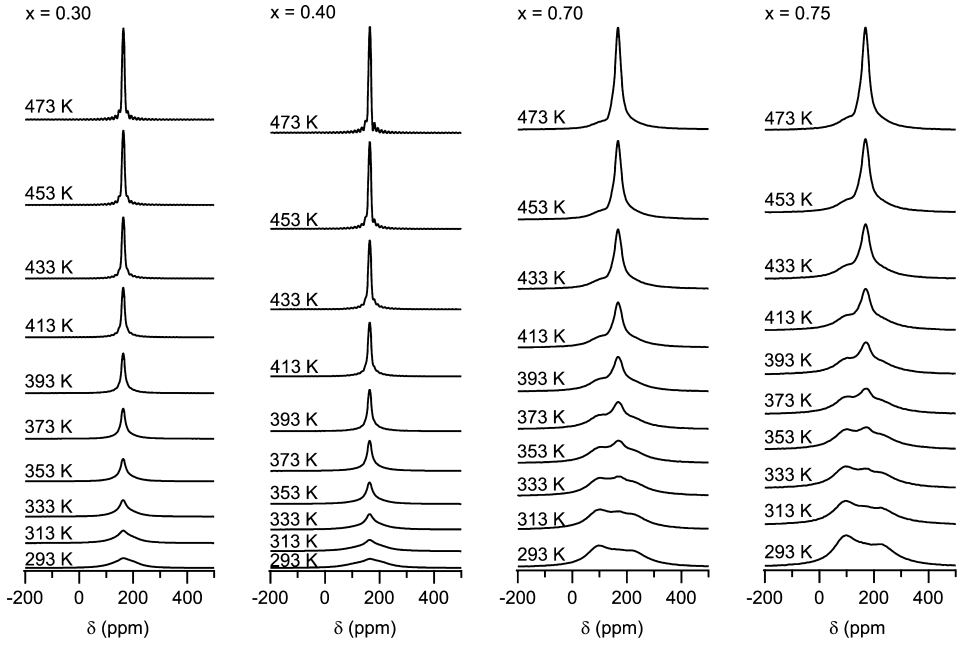

Figure 10. ^{19}F NMR spectra of the $Ba_{1-x}La_xF_{2+x}$ samples with $x = 0.30$, $x = 0.40$, $x = 0.70$, and $x = 0.75$ recorded at $\nu_0 = 376$ MHz at different temperatures.

it is hard to say which is the origin of this increase. However, due to the linear increase of A_0 it seems plausible to assume an increase of the particle density of mobile fluoride ions N with increasing x. No continuous change of the pre-exponential factor with x was observed for monocrystalline $Ba_{1-x}La_xF_{2+x}$ with $x \leq 0.50$ by Sorokin et al.[19] It should be noted that by keeping the value of the pre-exponential factor fixed to the value found for the sample with $x = 0.50$ the quality of the fittings of the Arrhenius plots is clearly reduced, and the behavior of the activation energy as a function of x is not changed significantly (not shown). Thus, the different conductivity behavior of the monocrystalline and the mechanosynthesized $Ba_{1-x}La_xF_{2+x}$ seems to be real.

The different conductivity behaviors of the mechanosynthesized $Ba_{1-x}La_xF_{2+x}$ and the monocrystalline material might be due to grain boundary effects as assumed by Rongeat et al.[47] In fact, the positions of the dc conductivity maxima seem to be in quite good agreement with the minima of the average crystallite size shown in Figure 3b. We will come back to this in the next section. To find an alternative explanation, it should be recalled that the PDF of the sample with $x = 0.70$ lacks a typical distance of the 2:2:2 clusters which, however, was observed in the PDFs of the samples with $x = 0.20$ and $x = 0.50$ (see section A). Hence, the decrease of the ionic conductivity between $x = 0.40$ and $x = 0.75$ might be due to a change of the microstructure of the grains or grain boundaries with x such that the migration enthalpy or defect formation enthalpy increases. Differing microstructures are often found for mechanically treated or synthesized compounds and their micro- or monocrystalline counterparts.[5] However, if the formation of percolation paths consisting of the distorted fluorite lattice close to the 2:2:2 clusters is assumed, a decrease of the conductivity is expected if the number of the presumed non- or badly conducting 2:2:2 clusters is increased beyond a certain number such that more and more paths are blocked by these clusters. Such behavior was, e.g., found for mixtures of the poor Li ion conductor Li_2O and the insulator B_2O_3.[57] In this context it should be recalled that the ^{19}F MAS NMR spectra showed a coalescence of the NMR line probably representing the fluoride ions in the 2:2:2 clusters for the samples with $x >$

dx.doi.org/10.1021/jp410018t | J. Phys. Chem. C XXXX, XXX, XXX−XXX

0.40 (see chapter B). However, a decrease of the ionic conductivity was not observed for monocrystalline $Ba_{1-x}La_xF_{2+x}$ up to $x \approx 0.50$. Kadlec et al.[16] assumed that this behavior may be explained by the assumption that the clusters formed are fragments of the tysonite structured fast fluoride ion conductor LaF_3 (see also ref 15) such that networks of these clusters should also show a good ionic conductivity. As already mentioned, Andersen et al.[13] found evidence that at least some of the fluoride ions in the 2:2:2 clusters are mobile.

Interestingly, the dc conductivity measured for the samples with $x = 0.90$ and $x = 0.85$ is approximately 1 order of magnitude smaller than reported by Reddy et al.[24] They also prepared $Ba_{1-x}La_xF_{2+x}$ with $1 \geq x \geq 0.85$ by high-energy ball milling. However, their compounds were prepared by milling in argon atmosphere and by using silicon nitride as a vial set material. Thus, the atmosphere, the mechanical energy, or the amount or kind of abraded material of the milling vial set introduced into the mixture seems to have an influence on the ion conductivity of tysonite-type $Ba_{1-x}La_xF_{2+x}$. Interestingly, the ionic conductivity of single crystals of $Ba_{1-x}La_xF_{2+x}$ crystallizing in the tysonite structure is even higher than reported by Reddy et al. for their mechanosynthesized samples.[24,58] They assumed that the decrease of the ionic conductivity is due to blocking grain boundaries.[47] In this context it might also be recapitulated that high-energy ball milling of LaF_3 did not increase its ionic conductivity compared to monocrystalline LaF_3. Thus, the introduction of defects or grain boundaries into tysonite structured $Ba_{1-x}La_xF_{2+x}$ due to mechanical stressing seems to impede the fluoride ion conductivity.

D. Static ^{19}F NMR. To gain information on the fluoride ion diffusion in $Ba_{1-x}La_xF_{2+x}$ from a microscopic point of view and to find answers to some of the questions raised by the results of the conductivity measurements, temperature-variable static ^{19}F NMR measurements were performed on all samples. In Figure 10 the ^{19}F NMR spectra of the $Ba_{1-x}La_xF_{2+x}$ samples with the highest ($x = 0.30$ and $x = 0.40$) and lowest ion conductivity ($x = 0.70$ and $x = 0.75$), in a temperature range from 293 to 473 K, are shown. The NMR lines of the samples with $x = 0.30$ and $x = 0.40$ consist of a single Lorentzian-shaped NMR line at 293 K, while the ones of the samples with $x = 0.70$ and $x = 0.75$ seem to be composed of at least two NMR lines. Furthermore, the NMR lines of the latter samples are much broader than those of the samples with $x = 0.30$ and $x = 0.40$. It should be mentioned that, expectedly, all the NMR lines are much broader than the NMR lines recorded under MAS conditions due to dipolar interactions of the fluoride ions. Moreover, it should be noted that the spectra of the samples investigated in a compositional range of $0.10 \leq x \leq 0.50$ are very similar to each other as well as the spectra of the samples with $0.60 \leq x \leq 0.80$ (see Figure S1, Supporting Information). The latter ones, however, show an increase of the line width with increasing x.

At a temperature of 313 K the spectra of the four samples shown in Figure 10 exhibit the emergence of a narrow NMR line atop the broad NMR line. This phenomenon is called motional narrowing in the case of the narrowing of a single NMR line and coalescence if two or more separated NMR lines fuse to a single, narrow NMR line. The origin of this effect is in both cases the same: the ions change their positions in the structure so fast that they lose their identity regarding their magnetic environment. Therefore, these ions experience an averaged magnetic environment and, thus, are represented by a single, narrow NMR line.[59] Motional narrowing can be observed if the jump frequency of the ion species investigated, or of the ions surrounding that species, becomes larger than the fwhm of the non-narrowed NMR line (Δ_{RL}). In the case of coalescence the jump rate has to be larger than the distance between the NMR lines which fuse to a single NMR line due to the exchange of fluoride ions between the sites represented by the initially separated NMR lines.[59] Thus, for the samples with $x = 0.30$ and $x = 0.40$ a jump rate of some of the fluoride ions exceeding $\Delta_{RL} = 46$ kHz at 313 K can be deduced from the spectra. For the narrow NMR line visible at $T \geq 313$ K in the spectra of the samples with $x = 0.70$ and $x = 0.75$ the calculation cannot be done since it is not clear which and how many NMR lines coalesce. The larger width of the narrow NMR line in the case of the samples with $0.60 \leq x \leq 0.80$ (fwhm $\approx$ 30 ppm at 473 K) compared to the ones of the samples with $x < 0.60$ (fwhm $\approx$ 10 ppm at 473 K) is probably due to a superposition of several narrow NMR lines with slightly different chemical shifts, thus originating from different NMR lines coalescing. This would mean that there is fast exchange of fluoride ions between more than one pair of chemically different fluoride ion sites. For comparison and completeness it should be noted that the NMR spectrum of BaF_2 consists of a single broad NMR line, and no change of the spectra with temperature up to 473 K was observed (not shown). The spectrum of LaF_3 (not shown) consists of two NMR lines at ambient temperature, exhibiting a narrow NMR line at temperatures larger than 333 K which is clearly narrower than the ones observed for the samples with $0.60 \leq x \leq 0.80$.

While for the samples with $x = 0.30$ and $x = 0.40$ a narrowing of the entire NMR line with increasing temperature can be observed until at a temperature of about 453 K only the narrow NMR line is left, in the case of the spectra of the other two samples shown in Figure 10, a broad NMR line is still visible beneath the narrow NMR line even at 473 K. Thus, the ratio of mobile fluoride ions to nonmobile or slow fluoride ions is clearly larger in the case of the samples with $x = 0.30$ and $x = 0.40$ than for the samples with $x = 0.70$ and $x = 0.75$ which may explain the decreased conductivity of the latter samples. Furthermore, there seem to be no nonmobile or even slow fluoride ions in the samples with $0.10 \leq x \leq 0.50$ at temperatures larger 453 K, although the fluoride ions in the 2:2:2 clusters, which seem to be present also in the mechanosynthesized $Ba_{1-x}La_xF_{2+x}$ (see sections A and B), were expected to be nonmobile at these temperatures.[18,21] In the case of percolation pathways between the fluorite-type structured material and the 2:2:2 clusters not all fluoride ions should be highly mobile but only the fluoride ions in the regions close to the 2:2:2 clusters. In that case a narrow line atop a broad NMR line would be observed even at 473 K (see, e.g., ref 60). However, also for the sample with $x = 0.10$ in which only a part of the material should be affected by the clusters a single narrow NMR line is obtained at 473 K (see Figure S4, Supporting Information). Thus, the percolation model outlined above seems inappropriate to describe the fluoride ion conductivity of the mechanosynthesized $Ba_{1-x}La_xF_{2+x}$ since the whole material seems to be highly conductive for the samples investigated with $x \leq 0.50$. Moreover, fluoride ions in the bulk and fluoride ions in the grain boundaries cannot be separated by their diffusivity for the samples with $x \leq 0.50$. If the increased ionic conductivity was caused by highly conducting grain boundaries, a narrow NMR line atop a broad NMR line representing the less good conducting bulk material should be observed. For the samples with $0.60 \leq x \leq 0.80$, however, the broad part of the NMR line

dx.doi.org/10.1021/jp410018t | J. Phys. Chem. C XXXX, XXX, XXX−XXX

might be associated with slow fluoride ions in the bulk and the narrow NMR line with fast fluoride ions in the grain boundaries. However, since the crystallite sizes for all $Ba_{1-x}La_xF_{2+x}$ samples investigated are quite similar it seems more likely that a change of the microstructure is responsible for the emergence of a broad NMR line beneath the narrow NMR line for the samples with $0.60 \leq x \leq 0.80$. This is also in accordance with the broadening of the narrow NMR line (vide supra) and the results discussed in section A. Wang et al.[50] reported that the mobility of the fluoride ions in the F1 sublattice of LaF_3 starts at lower temperatures and has a lower activation energy than the ones in the F2 and F3 sublattices. Therefore, the steady change of the character of the fluoride ion environments from the one at the fluorite and F1 sites toward the one of the F2/3 sites with increasing x might explain the decrease of the fluoride ion mobility.

In Figure 11 the chemical shifts of the maxima of the narrow NMR lines as a function of x are shown. The chemical shift

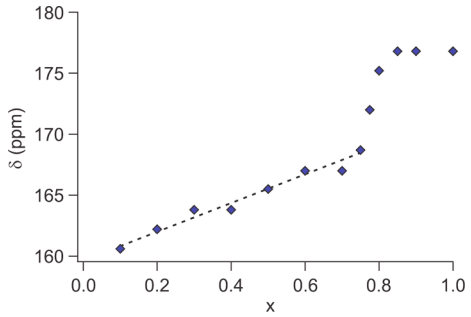

Figure 11. Change of the ^{19}F NMR istropic chemical shift of the narrow NMR line of the $Ba_{1-x}La_xF_{2+x}$ samples at 473 K, recorded at ν_0 = 376 MHz.

increases with x in an approximately linear fashion from x = 0.10 to x = 0.75. In the case of the tysonite structured $Ba_{1-x}La_xF_{2+x}$ the chemical shift values of the narrow NMR lines are very similar to the chemical shift value of the narrow NMR line in LaF_3, indicating similar transport mechanisms in these samples. Interestingly, the values of the chemical shifts of the narrow NMR lines of the samples with x = 0.75, x = 0.775, and x = 0.80 lie in-between the values of the chemical shifts of the narrow NMR lines of the samples with x = 0.70 (167 ppm) and x = 0.85 (177 ppm) (see Figure 11). Thus, there seems to be a smooth transition regarding the dynamic behavior of the fluoride ions when going from the fluorite to the tysonite structured $Ba_{1-x}La_xF_{2+x}$ reflecting the assumed continuous change from the fluorite to the tysonite structure.

IV. CONCLUSIONS

$Ba_{1-x}La_xF_{2+x}$ crystallizing in the cubic fluorite structure in the large range of $0 \leq x \leq 0.775$ was prepared by high-energy ball milling. A linear change of the lattice parameter a is observed for the samples in a range of $0 \leq x \leq 0.80$. $Ba_{1-x}La_xF_{2+x}$ with $0.55 < x < 0.80$ turned out to be metastable at ambient conditions and is, as already reported in different studies, most probably not accessible by conventional solid state synthesis.

By employing ^{19}F NMR, TEM, and X-ray total scattering, several indications for a continuous change from the fluorite to the tysonite structure by passing a structurally distorted crystalline phase were obtained. This transitional phase, found within a range from $x \approx 0.70$ to $x \approx 0.85$, combines structural aspects of both crystal structures.

The mechanosynthesized fluorite-type $Ba_{1-x}La_xF_{2+x}$ compounds show slightly higher dc conductivities for $x \leq 0.40$ than observed for the monocrystalline $Ba_{1-x}La_xF_{2+x}$ reported in the literature. In the case of the tysonite-type $Ba_{1-x}La_xF_{2+x}$ a pronounced decrease of the ionic conductivity with respect to the monocrystalline material was observed. A conductivity maximum for the fluorite-type material was found for $x \approx 0.40$. For compositions with $x > 0.40$ the ionic conductivity decreases until a conductivity minimum is reached for the sample with x = 0.75. The decrease of the ionic conductivity is accompanied by a change of the microstructure and diffusion behavior of the fluoride ions as well as a decrease of the ratio of highly mobile fluoride ions to nonmobile or slow moving fluoride ions.

For the samples with $0.10 \leq x \leq 0.50$ a high mobility of all fluoride ions at temperatures beyond 453 K in the $Ba_{1-x}La_xF_{2+x}$ was observed which means that (i) also the fluoride ions in the 2:2:2 clusters which seem to be present in the mechanosynthesized $Ba_{1-x}La_xF_{2+x}$ are highly mobile and (ii) the fluoride ion diffusivities in the bulk and the grain boundaries do not differ in a pronounced way. Thus, the enhanced ionic conductivity of the mechanosynthesized fluorite-type $Ba_{1-x}La_xF_{2+x}$ seems to be caused by the distorted fluorite lattice decreasing the migration or defect formation enthalpies for the fluoride ions in the whole material.

■ ASSOCIATED CONTENT

Supporting Information

Additional XRPD patterns, the PDFs plotted up to large r-values, Cole−Cole plots, and static ^{19}F NMR spectra of some of the samples. This material is available free of charge via the Internet at http://pubs.acs.org.

■ AUTHOR INFORMATION

Corresponding Authors

*Tel.: +49 511 7623187. E-mail: heitjans@pci.uni-hannover.de (P.H.).

*Tel: +49 511 7623273. E-mail: duevel@pci.uni-hannover.de (A.D.).

Notes

The authors declare no competing financial interest.

■ ACKNOWLEDGMENTS

We thank A. Feldhoff for the TEM measurements and E. Merzlyakova, W.-Y. Tsang, and A.-T. Duong for their support in sample preparation. We thank J. Caro for access to the Bruker Advance D8 diffractometer. We would like to thank I. Hanzu and M. Wilkening for valuable discussions and general help. Financial support by the Deutsche Forschungsgemeinschaft (DFG) within the frame of the Priority Program SPP 1415 is highly appreciated.

■ REFERENCES

(1) Heitjans, P.; Indris, S. Fast Diffusion in Nanocrystalline Ceramics Prepared by Ball Milling. *J. Mater. Sci.* **2004**, *39*, 5091−5096.

(2) Wilkening, M.; Epp, V.; Feldhoff, A.; Heitjans, P. Tuning the Li Diffusivity of Poor Ionic Conductors by Mechanical Treatment: High Li Conductivity of Strongly Defective $LiTaO_3$ Nanoparticles. *J. Phys. Chem. C* **2008**, *112*, 9291−9300.

(3) Ruprecht, B.; Wilkening, M.; Feldhoff, A.; Steuernagel, S.; Heitjans, P. High Anion Conductivity in a Ternary Non-Equilibrium Phase of BaF_2 and CaF_2 with Mixed Cations. *Phys. Chem. Chem. Phys.* **2009**, *11*, 3071−3081.

(4) Düvel, A.; Wilkening, M.; Uecker, R.; Wegner, S.; Šepelák, V.; Heitjans, P. Mechanosynthesized Nanocrystalline $BaLiF_3$: The Impact of Grain Boundaries and Structural Disorder on Ionic Transport. *Phys. Chem. Chem. Phys.* **2010**, *12*, 11251−11262.
(5) Šepelák, V.; Düvel, A.; Wilkening, M.; Becker, K.-D.; Heitjans, P. Mechanochemical Reactions and Syntheses of Oxides. *Chem. Soc. Rev.* **2013**, *42*, 7507−7520.
(6) Düvel, A.; Ruprecht, B.; Heitjans, P.; Wilkening, M. Mixed Alkaline-Earth Effect in the Metastable Anion Conductor $Ba_{1-x}Ca_xF_2$ ($0 \leq x \leq 1$): Correlating Long-Range Ion Transport with Local Structures Revealed by Ultrafast ^{19}F MAS NMR. *J. Phys. Chem. C* **2011**, *115*, 23784−23789.
(7) Düvel, A.; Wegner, S.; Efimov, K.; Feldhoff, A.; Heitjans, P.; Wilkening, M. Access to Metastable Complex Ion Conductors via Mechanosynthesis: Preparation, Microstructure and Conductivity of $(Ba,Sr)LiF_3$ with Inverse Perovskite Structure. *J. Mater. Chem.* **2011**, *21*, 6238−6250.
(8) Lyakhov, N.; Grigorieva, T.; Barinova, A.; Lomayeva, S.; Yelsukov, E.; Ulyanov, A. Nanosized Mechanocomposites and Solid Solution in Immiscible Metal Systems. *J. Mater. Sci.* **2004**, *39*, 5421−5423.
(9) Šepelák, V.; Becker, K.-D. Mechanochemistry: From Mechanical Degradation to Novel Materials Properties. *J. Korean Ceram. Soc.* **2012**, *49*, 19−28.
(10) Kuznetsov, S. V.; Fedorov, P. P. Morphological Stability of Solid-Liquid Interface During Melt Crystallization of $M_{1-x}R_xF_{2+x}$ Solid Solutions. *Inorg. Mater.* **2008**, *44*, 1434−1458.
(11) Sobolev, B. P.; Tkachenko, N. L. Phase Diagrams of BaF_2-(Y, Ln)F_3 Systems. *J. Less Common Met.* **1982**, *85*, 155−170.
(12) Kjems, J. K.; Andersen, N. H.; Schoonman, J.; Clausen, K. Structure and Dynamics of Disordered Solids - a Neutron-Scattering Study of $Ba_{1-x}La_xF_{2+x}$. *Phys. B&C* **1983**, *120*, 357−361.
(13) Andersen, N. H.; Clausen, K. N.; Kjems, J. K.; Schoonman, J. A Study of the Disorder in Heavily Doped $Ba_{1-x}La_xF_{2+x}$ by Neutron-Scattering, Ionic Conductivity and Specific-Heat Measurements. *J. Phys. C: Solid State Phys.* **1986**, *19*, 2377−2389.
(14) Cheetham, A. K.; Fender, B. E. F.; Steele, D.; Taylor, R. I.; Willis, B. T. M. Defect Structure of Fluorite Compounds Containing Excess Anions. *Solid State Commun.* **1970**, *8*, 171−173.
(15) Chernov, S. V.; Gunßer, W.; Murin, I. V. On Rare-Earth Clustering in Fluorite Type Solid Solutions MF_2-REF_3. *Solid State Ionics* **1991**, *47*, 67−70.
(16) Kadlec, F.; Simon, P.; Raimboux, N. J. Vibrational Spectra of Superionic Crystals $(BaF_2)_{1-x}(LaF_3)_x$. *Phys. Chem. Solids* **1999**, *60*, 861−866.
(17) Ivanov-Shits, A. K.; Sorokin, N. I.; Fedorov, P. P.; Sobolev, B. P. Specific Features of Ion Transport in Nonstoichiometric Fluorite-Type $Ba_{1-x}R_xF_{2+x}$ (R=La-Lu) Phases. *Solid State Ionics* **1989**, *31*, 269−280.
(18) Wapenaar, K. E. D.; van Koesveld, J. L.; Schoonman, J. Conductivity Enhancement in Fluorite-Structured $Ba_{1-x}La_xF_{2+x}$ Solid Solutions. *Solid State Ionics* **1981**, *2*, 145−154.
(19) Sorokin, N. I.; Breiter, M. W. Anionic Conductivity and Thermal Stability of Single Crystals of Solid Solutions Based on Barium Fluoride. *Solid State Ionics* **1997**, *99*, 241−250.
(20) Sorokin, N. I.; Sobolev, B. P. Nonstoichiometric Fluorides - Solid Electrolytes for Electrochemical Devices: A Review. *Crystallogr. Rep.* **2007**, *52*, 842−863.
(21) Wapenaar, K. E. D.; Schoonman, J. The Ionic Conductivity of Fluorite-Structured Solid Solutions of Composition: MF_2: UF_4: CeF_3 (M = Ca, Sr, Ba). *J. Electrochem. Soc.* **1979**, *126*, 667−672.
(22) Catlow, C. R. A. The Defect Properties of Anion-Excess Alkaline-Earth Fluorides. II. Intermediate and High Dopant Concentrations. *J. Phys. C* **1976**, *9*, 1859.
(23) Sorokin, N. I. Superionic Transport in Solid Fluoride Solutions with a Fluorite Structure. *Russ. J. Electrochem.* **2006**, *42*, 744−759.
(24) Anji Reddy, M.; Fichtner, M. Batteries Based on Fluoride Shuttle. *J. Mater. Chem.* **2011**, *21*, 17059−17062.
(25) Kennedy, J. H.; Hunter, J. C. Thin-Film Galvanic Cell $Pb/PbF_2/PbF_2$, CuF_2/Cu. *J. Electrochem. Soc.* **1976**, *123*, 10−14.
(26) Schoonman, J. A Solid-State Galvanic Cell with Fluoride-Conducting Electrolytes. *J. Electrochem. Soc.* **1976**, *123*, 1772−1775.
(27) Danto, Y.; Punjade, G.; Pistré, J. D.; Lucat, C.; Salardenne, J. A $Pb/PbF_2/BiF_3/Bi$ Thin Solid Film Reversible Galvanic Cell. *Thin Solid Films* **1978**, *55*, 347−354.
(28) Schoonman, J.; Wapenaar, K. E. D.; Oversluizen, G.; Dirksen, G. J. Fluoride-Conducting Solid Electrolytes in Galvanic Cells. *J. Electrochem. Soc.* **1979**, *126*, 709−713.
(29) Hagenmuller, P.; Réau, J.-M.; Lucat, C.; Matar, S.; Villeneuve, G. Ionic Conductivity of Fluorite-Type Fluorides. *Solid State Ionics* **1981**, *3/4*, 341−345.
(30) Schoonman, J.; Wolfert, A. Solid-State Galvanic Cells with Fast Fluoride Conducting Electrolytes. *Solid State Ionics* **1981**, *3/4*, 373−379.
(31) Kosacki, I. Physical Properties and Applications of $Cd_{1-x}Pb_xF_2$ Superionic Crystals. *Appl. Phys. A: Mater. Sci. Process.* **1989**, *49*, 413−424.
(32) Shareefuddin, M.; Jamal, M.; Narashima Chary, M. Solid State Battery with Pure and Doped Sodium Yttrium Fluoride as the Solid Electrolyte. *J. Phys. D: Appl. Phys.* **1995**, *28*, 440−442.
(33) Amatucci, G. G.; Prereira, N. Fluoride Based Electrode Materials for Advanced Energy Storage Devices. *J. Fluorine Chem.* **2006**, *128*, 243−262.
(34) West, W.; Whitacre, J.; Del Castillo, L. Solid State Fluoride Battery for High Temperature Applications. *Electrochemical Society Meeting*, May 2007, Chicago, IL.
(35) Bouazza, S.; Saberi, A.; Willert-Porada, M. Preparation and Electrochemical Properties of Nano-Sized SnF_2 as Negative Electrode for Lithium-Ion Batteries. *Mater. Lett.* **2011**, *65*, 1334−1336.
(36) Bonne, R. W.; Schoonman, J. Electrode Processes of Lead Halides: Part 2: β-PbF_2. *J. Electrochem. Soc.* **1978**, *125*, 1628−1632.
(37) Stefan, I. C.; Jacobson, C. P.; Visco, S. J.; De Jonghe, L. C. Solid-State Electrochemistry of Fluoride Ionic Conductive Materials. *Electrochemical Society Meeting*, October 2004, Honolulu, HI.
(38) Hanzu, I.; Düvel, A.; Preishuber-Pflügel, F.; Heitjans, P.; Wilkening, M. unpublished results.
(39) Hammersley, A. P.; Svensson, S. O.; Hanfland, M.; Fitch, A. N.; Häusermann, D. Two-Dimensional Detector Software: From Real Detector to Idealised Image or Two Theta Scan. *High Press. Res.* **1996**, *14*, 235.
(40) Qiu, X.; Thompson, J. W.; Billinge, S. J. L. PDFgetX2: A GUI-Driven Program to Obtain the Pair Distribution Function from X-Ray Powder Diffraction Data. *J. Appl. Crystallogr.* **2004**, *37*, 678−678.
(41) *Diffusion in Condensed Matter - Methods, Materials, Models*; Heitjans, P., Kärger, J., Eds.; Springer: Berlin, 2005.
(42) Fukushima, E.; Roeder, S. B. W. *Experimental Pulse NMR*; Addison-Wesley: Reading, MA, 1981.
(43) Stanley, P. D. *Organofluorines*; Neilson, A. H., Ed.; Springer-Verlag: Berlin Heidelberg, 2002; p 12.
(44) Bednarcik, J.; Michalik, S.; Kolesar, V.; Rütt, U.; Franz, H. In Situ XRD Studies of Nanocrystallization of Fe-Based Metallic Glass: A Comparative Study by Reciprocal and Direct Space Methods. *Phys. Chem. Chem. Phys.* **2013**, *15*, 8470−8479.
(45) Williamson, G. K.; Hall, W. H. X-Ray Line Broadening from Filed Aluminium and Wolfram. *Acta Metall.* **1953**, *1*, 22−31.
(46) Youngman, R. E.; Smith, C. M. Multinuclear NMR Studies of Mixed $Ca_{1-x}Sr_xF_2$ Crystals. *Phys. Rev. B* **2008**, *78*, 014112−1−014112−6.
(47) Rongeat, C.; Anji Reddy, M.; Witter, R.; Fichtner, M. Nanostructured Fluorite-Type Fluorides as Electrolytes for Fluoride Ion Batteries. *J. Phys. Chem. C* **2013**, *117*, 4943−4950.
(48) Seifert, K.-F. Untersuchungen zur Druck-Kristallchemie der AX_2-Verbindungen. *Fortschr. Miner.* **1968**, *45*, 214−280.
(49) Leger, J. M.; Haines, J.; Atouf, A.; Schulte, O. High-Pressure X-Ray and Neutron-Diffraction Studies of BaF_2: An Example of a Coordination Number of 11 in AX_2 Compounds. *Phys. Rev. B* **1995**, *52*, 13247−13256.

(50) Wang, F.; Grey, C. P. Probing the Mechanism of Fluoride-Ion Conduction in LaF_3 and Strontium-Doped LaF_3 with High-Resolution ^{19}F MAS NMR. *Chem. Mater.* **1997**, *9*, 1068−1070.
(51) Maximov, B.; Schulz, H. Space Group, Crystal Structure and Twinning of Lanthanum Trifluoride. *Acta Crystallogr.* **1985**, *B41*, 88−91.
(52) Bureau, B.; Silly, G.; Buzaré, J. Y.; Emery, J. Superposition Model for ^{19}F Isotropic Chemical Shift in Ionic Fluorides: From Basic Metal Fluorides to Transition Metal Fluoride Glasses. *Chem. Phys.* **1999**, *249*, 89−104.
(53) Duer, M. J. *Introduction to Solid-State NMR Spectroscopy*; Blackwell Publishing Ltd.: U.K., 2004; p 116ff.
(54) Heitjans, P.; Indris, S. Diffusion and Ionic Conduction in Nanocrystalline Ceramics. *J. Phys.: Condens. Matter* **2003**, *15*, R1257−R1289.
(55) Puin, W.; Rodewald, S.; Ramlau, R.; Heitjans, P.; Maier, J. Local and Overall Ionic Conductivity in Nanocrystalline CaF_2. *Solid State Ionics* **2000**, *131*, 159−164.
(56) Sinitsyn, V. V.; Lips, O.; Privalov, A. F.; Fujara, F.; Murin, I. V. Transport Properties of LaF_3 Fast Ionic Conductor Studied by Field Gradient NMR and Impedance Spectroscopy. *J. Phys. Chem. Solids* **2003**, *64*, 1201−1205.
(57) Indris, S.; Heitjans, P.; Roman, H. E.; Bunde, A. Nanocrystalline versus Microcrystalline $Li_2O:B_2O_3$ Composites: Anomalous Ionic Conductivities and Percolation Theory. *Phys. Rev. Lett.* **2000**, *84*, 2889−2892.
(58) Roos, A.; Schoonman, J. Electronic Conductivity in $La_{1-x}Ba_xF_{3-x}$ Crystals. *Solid State Ionics* **1984**, *13*, 205−211.
(59) Duer, M. J. *Introduction to Solid-State NMR Spectroscopy*; Blackwell Publishing Ltd.: U.K., 2004; p 295ff.
(60) Heitjans, P.; Indris, S.; Wilkening, M. In *Nanocomposites: Ionic Conducting Materials and Structural Spectroscopies*; Knauth, P., Schoonman, J., Eds.; Springer: Berlin, 2008, pp 227−246.